Proceedings of the 4th WSEAS International Conference on Fluid Mechanics and Aerodynamics, Elounda, Greece, August 21-23, 2006 (pp343-348)

Numerical Simulation of Transient Flow and Head Distribution through a Single Blade Centrifugal Pump Impeller

JOHN DALY, BRIAN DE SOUZA, ANDREW NIVEN and PATRICK FRAWLEY
John Holland Research Centre
Department of Mechanical and Aeronautical Engineering
University of Limerick
IRELAND

Abstract: - The analysis of the transient head and flow distribution through a single blade centrifugal pump impeller using computational fluid dynamics is presented. The hydraulic performance is characterised by significant fluctuations in head and required power with each revolution. This research investigates the source of the head fluctuations and the transient nature of the flow field. The analysis shows very significant variation in head, radial velocity and velocity outlet angle with angular position for any given impeller position.

Key-Words: - Single-blade, single-channel, centrifugal, impeller, unsteady, hydraulic

1 Introduction

The design of a centrifugal pump impeller is fundamentally based on the Euler Equation, which allows prediction of the theoretical pump performance. Conventional design methods, such as those of Stepanoff (1957) or Lazarkiewicz and Troskolanski (1965) predict real pump performance through the use of slip factors as provided by Busemann (1928) or Pfleiderer (1924) for example.

The design of centrifugal pump impellers for wastewater applications involves significant deviation from conventional impeller design methods. Due to the capability requirement of pumping unscreened contaminated water without clogging, it is necessary that wastewater pump impellers have a much larger channel size than would be required for a conventional impeller operating at the same head and flow conditions.

The increased channel size requirements are so severe that wastewater pump impellers normally have only one or two blades. In addition the blade outlet height is quite often two to three times greater than for a conventional impeller design. The use of one or two blades represents an extreme deviation from the theoretical assumption of an infinite number of blades on which the Euler equation is based. The increased blade outlet height results in a much lower radial velocity, and consequently a lower fluid outlet angle from the impeller region.

With such a small number of blades and the large blade height the fluid receives much less guidance from the impeller than with a conventional design and, as a result, significant three-dimensional flow patterns exist. The purpose of this paper is to present an overview of the numerical predictions of these three dimensional flow patterns for a single blade impeller.

2 Model Description

2.1 Physical Geometry

The results presented are from the numerical analysis of an impeller, shown in Fig. 1, with a medium specific speed (Ns = 58). The impeller diameter was 235mm while the blade outlet height was 95mm. The impeller and volute geometry were generated using the SolidWorks™ CAD package before creation of the fluid domains for the inlet, impeller and volute sections.

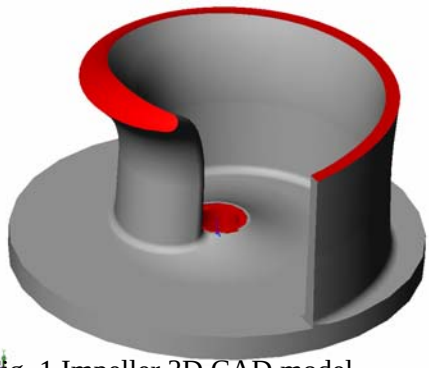

Fig. 1 Impeller 3D CAD model

2.2 Grid Generation

The Ansys ICEM CFD 5.1 package was used for the grid generation. The computational domain

was meshed as three separate regions: an inlet, the impeller and the volute regions. The impeller and volute regions are shown in Fig. 2. The use of three separate regions allowed specification of the impeller region as a rotating domain. A hybrid type mesh was used for all three domain regions, consisting of 5 layers of prism cell on the surfaces and tetrahedral cells for the remainder of the domain volume. A total of 1035k cells were used, of which 744k were tetrahedral and 291k were prism cells.

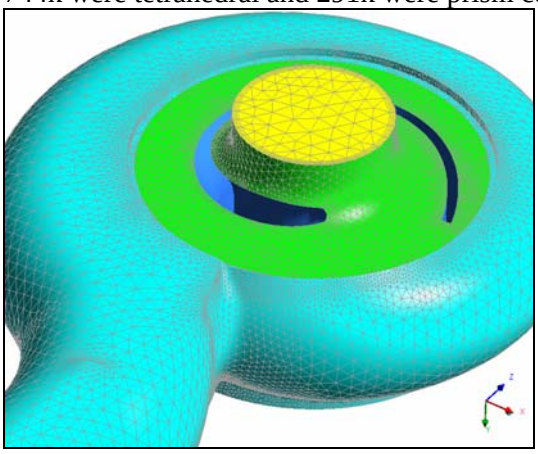

Fig. 2 Impeller and volute regions of the computational domain

2.3 Computational Model

The model was analysed using the Ansys CFX 5.7.1 numerical code. The flow was modelled as turbulent incompressible, and a full transient simulation was conducted for ten revolutions, with a time step size corresponding to a rotation angle of six degrees. The turbulence model used was the standard k-ε model while the wall boundary layers were modeled using a log-law scalable wall-function approach. All walls throughout the domain were modeled with a no-slip boundary condition. The analysis used a second order backward Euler implicit transient time stepping scheme. The grid generation and computational model are described in more detail by De Souza et. al. (2006).

3 Results Analysis

3.1 Hydraulic Performance

The transient torque and outlet head predictions for the final three revolutions at the best efficiency flow rate are shown in Fig. 3. The x-axis represents the impeller angular position in terms of number of revolutions, where each revolution in counted when the impeller trailing edge passes the volute cutwater. Fig. 3 shows that there is significant fluctuation in both the head and torque predictions as the impeller rotates, with the minimum head occurring when the impeller trailing edge has just passed the cutwater. The maximum head occurs at the ¾ revolution point, i.e. when the impeller trailing edge is at –90° to the cutwater. The amplitude of the pressure fluctuation was found to be approximately 40% of the average head. Similar results for fluctuation magnitude and position of minimum and maximum head were found by Benra et. al. (2004) at the nominal flowrate for a single blade, closed (i.e. integral shroud) impeller.

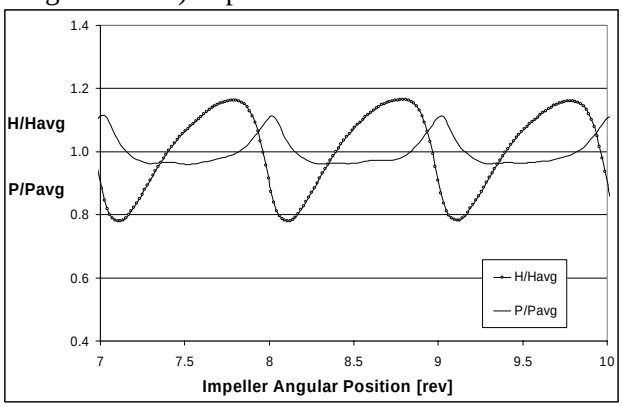

Fig. 3 Transient head and torque predictions at best efficiency flow rate

Using the average of the transient results for the final two revolutions, the hydraulic performance curves of the pump were plotted. These are shown in non-dimensional form in Fig. 4. The predicted best efficiency point is at 1.25 times the design flow rate, while the predicted peak power occurs at 1.5 times the design flow rate.

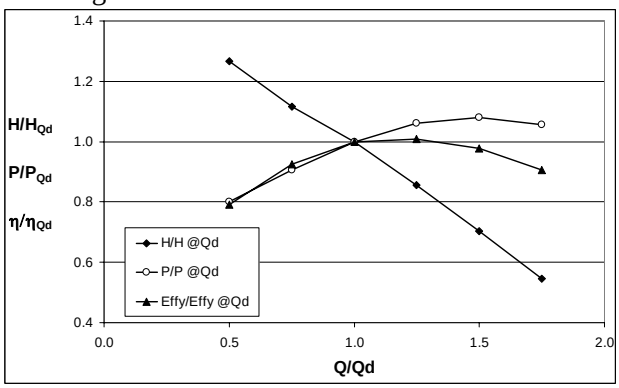

Fig. 4 Non-dimensional hydraulic performance

3.2 Fluid Flow Analysis

The fluid flow analysis is displayed in the following sections as vector and contour plots on two planes; the first perpendicular to the impeller rotation axis and at an axial distance corresponding to the blade mid-height point and the second a cylindrical surface with a diameter equal to the impeller diameter.

3.2.1 Head predictions

Fig. 5 to Fig. 8 show contours of non-dimensional head on the 50% blade height plane at 90° intervals. The values of head are based on the static pressure relative to the pump inlet and are non-dimensionalised by the head obtained at the outlet, averaged over two revolutions.

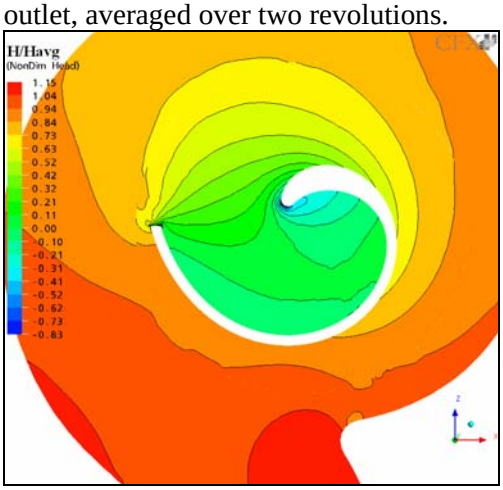

Fig. 5 Non-dimensional head contours with impeller at 270° (Q = Q_{BEP}, plane @ 50% blade height)

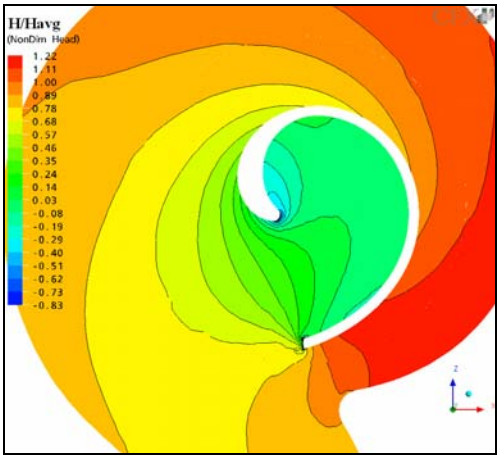

Fig. 6 Non-dimensional head contours with impeller at 0° (Q = Q_{BEP}, plane @ 50% blade height)

At any given impeller position there is obviously a significant variation in the pressure field throughout both the impeller and volute regions. The single blade sets up a rotating high pressure region which precedes the trailing edge by 30 – 90° and a corresponding low pressure region following the trailing edge. This rotating pressure field within the impeller region does not vary significantly with impeller position, however it is the high and low pressure zones passing the volute outlet which give rise to the previously observed pressure pulses. Although the highest pressure value is observed in Fig. 6, the contours in the volute outlet region indicate that the head is 0.68 to 0.89 times the average head, corresponding to Fig. 3 for this impeller position. The rotating pressure field within the volute, and the impeller positions corresponding to the head fluctuations correspond well with those reported by Benra et. al (2005). In particular, the increase in head when the blade trailing edge approaches the cutwater and the reduction in head when it passes the cutwater agree very well.

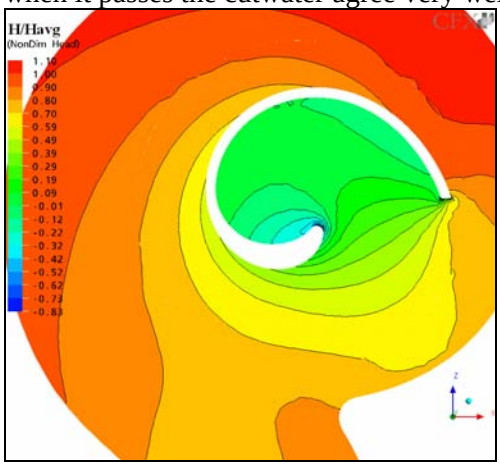

Fig. 7 Non-dimensional head contours with impeller at 90° (Q = Q_{BEP}, plane @ 50% blade height)

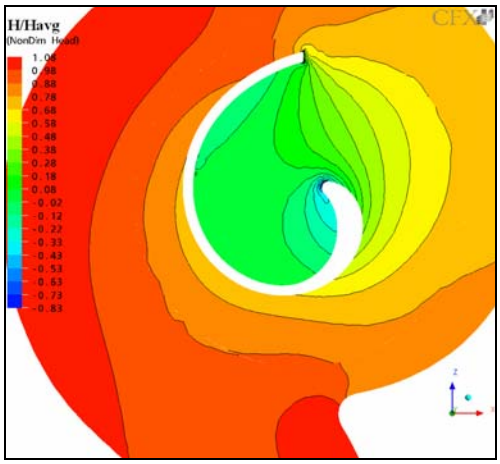

Fig. 8 Non-dimensional head contours with impeller at 180° (Q = Q_{BEP}, plane @ 50% blade height)

3.2.2 Velocity predictions

Vectors and contours of relative velocity for the impeller region are shown in Fig. 9 to Fig. 11. As with the contours of head, a relatively constant velocity field appears to rotate with the impeller. The most significant change was the increase in velocity magnitude at the trailing edge as it passes the cutwater. At any given impeller position there is considerable distortion in the velocity contours near the blade trailing edge. Away from the wake area the relative velocity magnitude along the impeller region boundary appears constant at ~80% of the peak value.

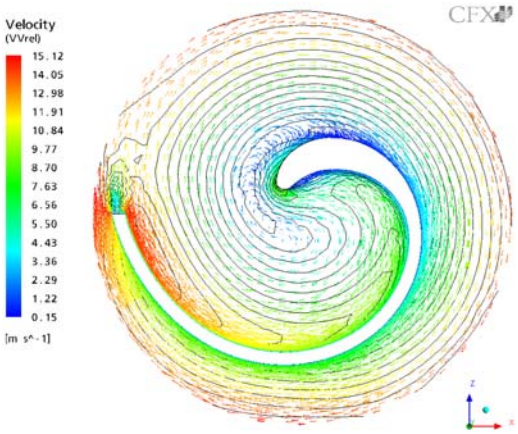

Fig. 9 Relative velocity with impeller at 270° (Q = Q_{BEP}, plane @ 50% blade height)

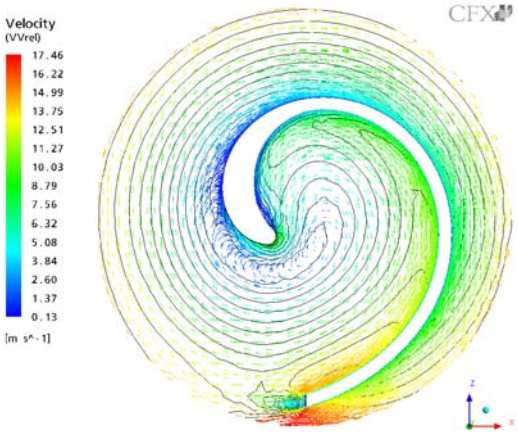

Fig. 10 Relative velocity with impeller at 0° (Q = Q_{BEP}, plane @ 50% blade height)

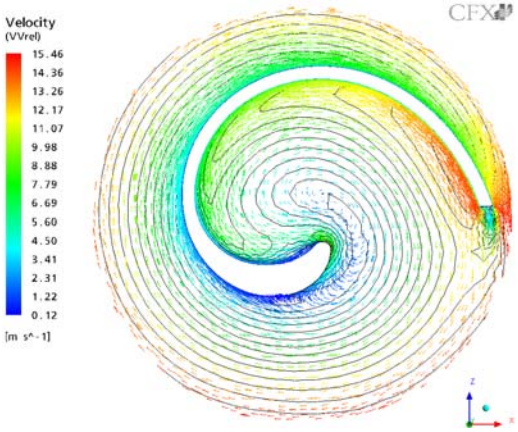

Fig. 11 Relative velocity with impeller at 90° (Q = Q_{BEP}, plane @ 50% blade height)

The velocity vectors show that the stagnation point occurs at a significant distance along the pressure surface from the leading edge. This gives rise to a small separated region inside the leading edge and is probably caused by the relatively small inner diameter of the blade at this height. Fig. 12 shows that the separated region inside the leading edge is significantly worse nearer the blade hub.

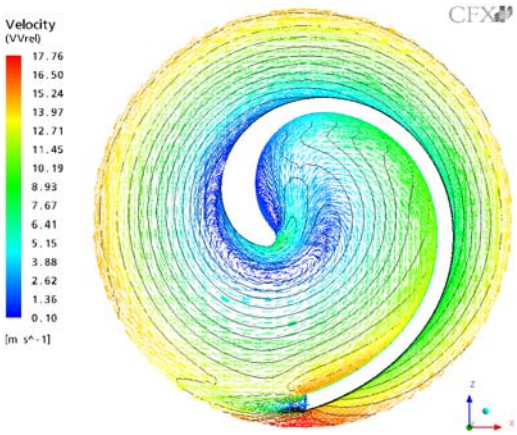

Fig. 12 Relative velocity with impeller at 0° (Q = Q_{BEP}, plane @ 15% blade height)

Although the relative velocity magnitude at the impeller outer diameter appears constant away from the trailing edge region, it is the radial velocity and the velocity angle that is of most interest from a pump design perspective.

Fig. 13 and Fig. 16 show the radial velocity vectors and contours on a cylindrical surface, described by the rotation of the trailing edge, for the impeller at the cutwater and directly opposite respectively. These plots show that there is significant variation in radial velocity with angular position from the trailing edge, regardless of impeller position relative to the cutwater. As the flow approaches the trailing edge the radial velocity increases, with the strongest radial flow occurring in a band along the trailing edge. For the remainder of the surface the radial flow is quite small, and in some places actually reverses direction. The variation in the radial velocity component on this surface is greater than that published for multi-bladed impellers. For example, Hergt et. al. (2004) show almost as much variation in the radial velocity as found here, but also shows that, at the design flow rate, the variation in meridional velocity at the entrance to the volute occurs in the axial direction, rather than in the circumferential direction.

Fig. 15 plots the head development for the same surface and this shows that there is a gradual and steady increase in the static head from the lowest point near the trailing edge wake around the surface back to the trailing edge itself. Fig. 14 and Fig. 17 show the corresponding velocity angle contours, normalised using the impeller outlet angle, β2. As expected, the velocity angle contours correspond closely to the radial velocity vectors, and indicate significant variation over the surface shown. It is only in the narrow band along the trailing edge span where the radial velocity was largest that the velocity angle approaches the magnitude of the

blade outlet angle. For much of the surface shown it is less than 25% of the blade outlet angle.

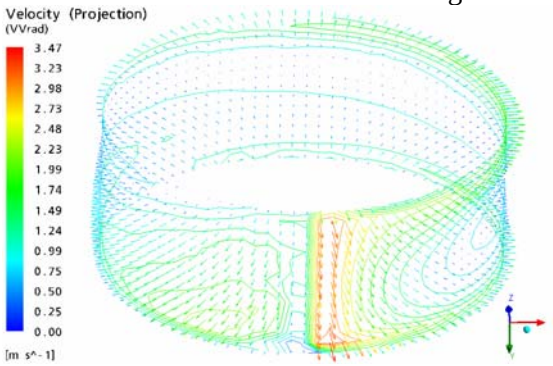

Fig. 13 Meridional velocity for impeller @ 0° (Q = Q_{BEP}, plane @ r = Impeller Radius)

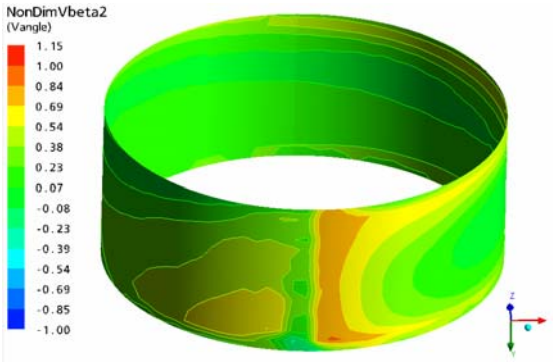

Fig. 14 Normalised velocity angle for impeller @ 0° (Q = Q_{BEP}, plane @ r = Impeller Radius)

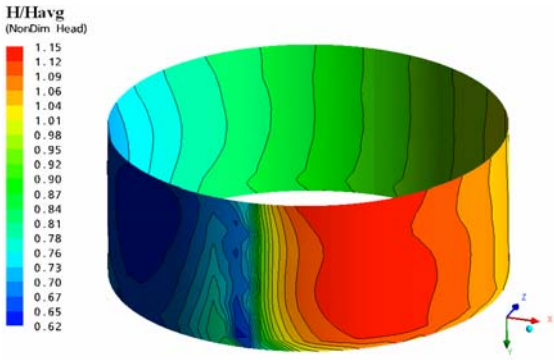

Fig. 15 Non-dimensional head for impeller @ 0° (Q = Q_{BEP}, plane @ r = Impeller Radius)

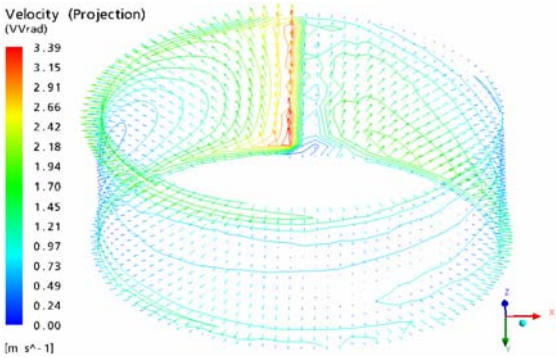

Fig. 16 Meridional velocity for impeller @ 180° (Q = Q_{BEP}, plane @ r = Impeller Radius)

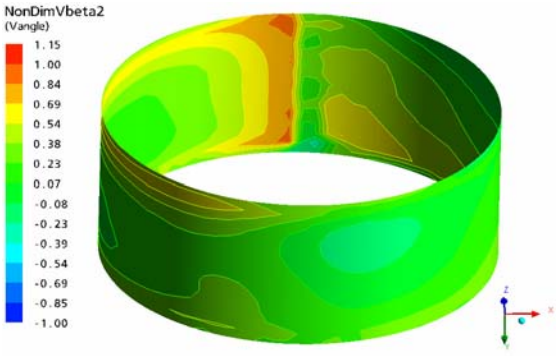

Fig. 17 Normalised velocity angle @ 180° position (Q = Q_{BEP}, plane @ r = Impeller Radius)

3.2.3 Fluid Outlet Angle

The distribution of the normalised velocity angle on the cylindrical surface is shown in more detail in Fig. 18 to Fig. 20 for the –90°, 0° and +90° impeller positions. The legend in each plot indicates the axial distance from the blade hub as a ratio of the overall blade height. For Fig. 18 the impeller trailing edge was at 270° (i.e. –90° from the cutwater).

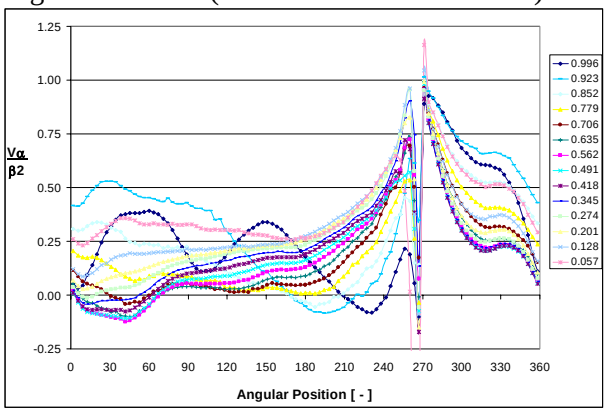

Fig. 18 Normalised velocity angle @ 270° position (Q = Q_{BEP}, plane @ r = Impeller Radius)

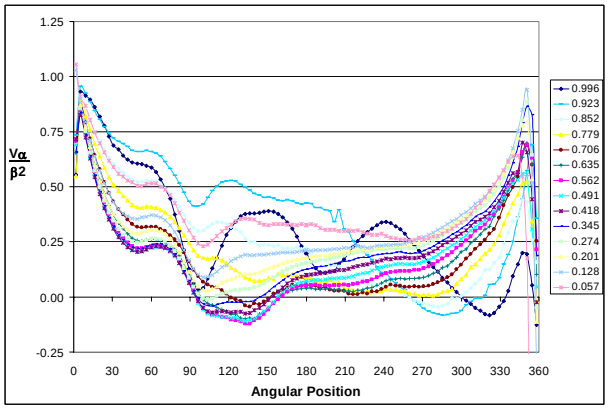

Fig. 19 Normalised velocity angle @ 0° position (Q = Q_{BEP}, plane @ r = Impeller Radius)

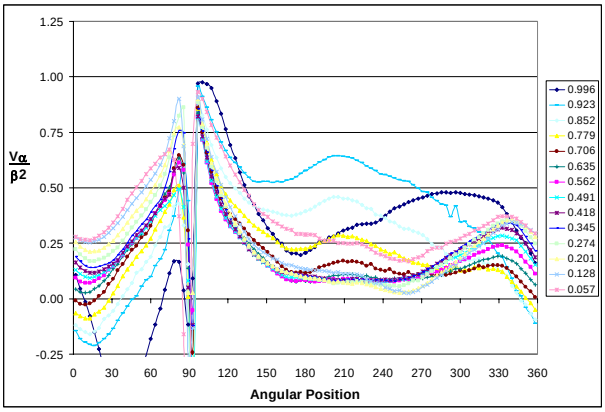

Fig. 20 Normalised velocity angle @ 90° position (Q = Q_{BEP}, plane @ r = Impeller Radius)

For each of the plots shown in Fig. 18 to Fig. 20 the peak velocity angle occurs at the trailing edge, followed immediately by the negative spike from the trailing edge wake. Ignoring the wake, it can be seen that there is a region ± 75° from the trailing edge where the velocity angle rises to near the blade outlet angle value and then falls again. This is shown more clearly in Fig. 21 which plots the average normalised velocity angle at each angular position for the -90°, 0°, 90° and 180° impeller positions. The peak value of the average velocity angle is lower at the 0° and 90° positions, possibly due to the influence of the cutwater and the high pressure region shown in Fig. 6.

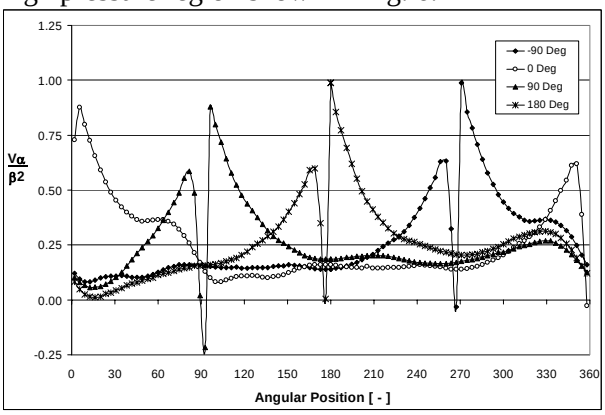

Fig. 21 Average normalised velocity angle for impeller @ -90°, 0°, 90° and 180° (Q = Q_{BEP}, plane @ r = Impeller Radius)

4 Conclusions

This research investigates the transient nature of the flow field within a single channel impeller pump. It shows how the rotating pressure field within the impeller region results in significant fluctuations in the outlet head. The research also highlights the significant variations in radial velocity and velocity angle, showing that the fluid exit angle only approaches the blade outlet angle for a narrow region along the impeller trailing edge.

Acknowledgement

This work has been funded by ABS Pumps (Ireland) Ltd. and Enterprise Ireland.

Nomenclature

H	= Head
N	= Rotational rate
N_s	= Specific Speed ($NQ^{1/2}/H^{3/4}$)
P	= Power
Q, Qd, Q_{BEP}	= Flowrate, Design flowrate, Flowrate at best efficiency point
r	= radius
Vα	= Velocity angle
β2	= Blade outlet angle
η	= Efficiency

References:

[1] Benra, F.K., Dohmen, H.J. and Sommer, M., *Periodic Unsteady Flow in a Single-Blade Centrifugal Pump – Numerical and Experimental Results*, Proc. of FEDSM2005, ASME Fluids Engineering Division Summer Meeting and Exhibition, Houston, TX, USA, 2005

[2] Benra, F.K., Sommer, M., Müller, M. and Töws, A., *Investigation of the Three-Dimensional Time Accurate Flow in a Single-Blade Sewage Water Pump*, Paper No. 61, 4th South African Conf. on Applied Mechanics, Johannesburg, South Africa, 2004

[3] Busemann, A., *Das Förderhöhenverhältniss Radialer Kreiselpumpen Mit Logarithisch-spiraligen Schauflen*, Z. Angew Math. Mech, 1928, pp.371 – 381

[4] De Souza, B., Daly, J., Niven, A. and Frawley, P., *Numerical Simulation of Transient flow through Single Blade Centrifugal Pump Impellers with Tipgap Leakage*, submitted to 4th IASME / WSEAS Int. Conf. on Fluid Mechanics and Aerodynamics, Crete, 2006

[5] Hergt, P., Meschkat, S. and Stoffel, B., *The Flow and Head Distribution within the Volute of a Centrifugal Pump in comparison with the Characteristics of the Impeller without Casing*, Jnl. Computational and Applied Mechanics, Vol. 5, No. 2, 2004, pp. 275 – 285

[6] Lazarkiewicz, S. and Troskolanski, A. T, *Impeller Pumps: Selection, Systems and Application*, Pergamon Press, 1965

[7] Pfleiderer, C., Die Kreiselpumpen fur Flussigkeiten und Gase, 1st Ed., Springer, Berlin, 1924

[8] Stepanoff, A.J, Centrifugal and Axial Flow Pumps: Theory, design and Application, 2nd Ed., Chapman and Hall, 1957